












Electroacupuncture Regulates Mitochondria-Endoplasmic Reticulum interactions via *Fnl* in a Parkinson's Disease Model: Transcriptomic Evidence

Peilin Lyu¹, Feng Wen¹, Zhiyi Fu¹, Junying Li¹, Qiyan Li¹, Xiaowen Cai¹,
Shengtao Huang¹, Xiaoke Qiu¹, Zhinan Zhang¹, Yong Huang^{1,2,3,*},
Jiping Zhang^{1,3,4,*}

¹School of Traditional Chinese Medicine, Southern Medical University, 510000 Guangzhou, Guangdong, China

²Nanfang Hospital, Southern Medical University, 510000 Guangzhou, Guangdong, China

³Guangdong Basic Research Center of Excellence for Integrated Traditional and Western Medicine for Qingzhi Diseases, 510000 Guangzhou, Guangdong, China

⁴Zhujiang Hospital, Southern Medical University, 510000 Guangzhou, Guangdong, China

*Correspondence: nanfanglihuang@163.com (Yong Huang); zhangjp611@163.com (Jiping Zhang)

Academic Editors: Gernot Riedel and Bettina Platt

Submitted: 1 May 2025 Revised: 17 July 2025 Accepted: 21 July 2025 Published: 18 September 2025

Abstract

Aims: Parkinson's disease (PD) is characterized by dopaminergic neuron degeneration and disruption to mitochondria-associated endoplasmic reticulum membranes (MAMs). This study explores whether electroacupuncture (EA) can alleviate 1-methyl-4-phenyl-1,2,3,6-tetrahydropyridine (MPTP) induced PD symptoms and investigates the underlying mechanisms using RNA sequencing (RNA-seq). **Methods:** A PD mouse model was established using MPTP, followed by EA treatment at governing vessel 20 (GV20) and gallbladder meridian 34 (GB34) acupoints, with sham EA treatments as a control. Behavioral assays, immunohistochemistry, and Western blotting assessed neuroprotective effects. MAM integrity was assessed using Western blot, immunofluorescence staining, and transmission electron microscopy. RNA-seq and protein-protein interaction (PPI) analysis identified differentially expressed genes which were validated by real-time fluorescence quantitative polymerase chain reaction (qRT-PCR). **Results:** EA treatment improved motor performance, increased substantia nigra (SN) and striatum tyrosine hydroxylase expression, reduced SN alpha-synuclein, and improved SN dopamine neuron MAM structure. Transcriptomic analysis identified 32 MAM-associated genes, of which fibronectin-1 (*Fnl*) was identified as a key regulator. EA was found to upregulate *Fnl* expression, suggesting its involvement in MAM stabilization and neuroprotection. **Conclusion:** EA at GV20 and GB34 alleviated motor and neural impairments in a PD mouse model potentially through modulation of *Fnl* and its role in MAM-associated pathways.

Keywords: electroacupuncture; *Fnl*; mitochondria-associated membranes; Parkinson's disease; RNA sequence analysis

1. Introduction

Parkinson's disease (PD), a widespread degenerative disorder of the central nervous system, is characterized by degeneration of dopaminergic neurons in the substantia nigra (SN), alpha-synuclein (α -syn) aggregation and Lewy body formation [1]. Its incidence is 3.9% in China and 1–2% globally [2,3]. PD primarily presents with motor and non-motor symptoms (for example bradykinesia, tonic, resting tremor, dysphagia and dyspnea). Its pathogenesis is extremely complex, involving iron depletion, aberrant α -syn accumulation, oxidative stress, mitochondrial dysfunction, neuroinflammation and gut microbiota dysregulation. The interplay among these mechanisms further complicates PD pathogenesis and treatment [4]. Currently, there are limited effective treatments for PD, mainly drug treatment using compounded levodopa and dopamine (DA) receptor agonists [5], which themselves have limitations. For example, long-term use of levodopa often leads to levodopa-induced dyskinesias [6].

Acupuncture has become a widely used complementary therapy for the treatment of neurological disorders including PD [7,8]. Clinical investigations have demonstrated that the concurrent application of electroacupuncture (EA) and medication significantly improves motor symptoms such as myotonia, bradykinesia and resting tremor in patients with PD when compared to medication alone [9,10]. EA has been shown to inhibit apoptosis, upregulate neurotrophic factors and activate phosphatidylinositol 3-kinase/protein kinase B (PI3K/Akt) and mitogen-activated protein kinase kinase/extracellular signal-regulated kinase (MEK/ERK) pathways, to promote dopaminergic neuron survivals in PD [11]. EA targeting specific brain regions activates Akt and brain-derived neurotrophic factor (BDNF), increasing striatal DA phosphatase-interacting protein levels and reducing 1-methyl-4-phenyl-1,2,3,6-tetrahydropyridine (MPTP)-induced symptoms [12]. It also upregulates BDNF expression to counteract neurotoxicity and prevent

reductions in BDNF and phosphorylated-ERK levels in the striatum (STR) [13]. EA modulates inflammation and brain connectivity, potentially improving PD symptoms through vagal anti-inflammatory activation and enhanced brain function [14]. Acupoints governing vessel 20 (GV20) and gallbladder meridian 34 (GB34) have significant potential to alleviate clinical symptoms of PD [15–18]. EA in PD model rats has been shown to increase DA levels in STR, inhibit cell apoptosis in the SN and reduce the loss of dopaminergic neurons [19]. Overall, EA improves dopaminergic neuron survival, protecting against neuronal fiber loss in PD [8,20].

Mitochondria-associated endoplasmic reticulum membranes (MAMs) are specialized junctions between the outer mitochondrial membrane and the endoplasmic reticulum (ER) membrane, facilitating complex interactions between these two organelles [21]. MAMs significantly contribute to PD pathogenesis. The study has shown that after transfection of α -syn and its mutants into SH-SY5Y cells, α -syn accumulates on the outer mitochondrial membrane and co-localizes with MAMs [22]. This accumulation increases the distance between the ER and mitochondria, disrupting their coupling, which impairs Ca^{2+} exchange and mitochondrial adenosine triphosphate (ATP) production between the two organelles and may contribute to mitochondrial dysfunction in PD [23]. α -syn, enriched presynaptically and perinuclearly, regulates Ca^{2+} delivery to MAMs via recombinant vesicle associated membrane protein associated protein B (VAPB) binding, affecting mitochondrial ATP production and synaptic activity. Loss of synaptic function, critical in PD, is influenced by VAPB protein tyrosine phosphatase-interacting protein 51-mediated MAMs in the synaptic region rich in ER and mitochondria [24,25]. In PD, a defect in the ubiquitin E3 ligase Parkin can lead to non-ubiquitination of mitofusin 2 (Mfn2), resulting in reduced tight junctions between the ER and mitochondria and reduced mitochondrial Ca^{2+} uptake [26]. The PD protein parkinsonism-associated deglycase (DJ-1) is a component of the inositol1,4,5-trisphosphate receptors-glucose-regulated protein 75-voltage dependent anion channel 1 complex. Disruption of the mitochondria-ER tethering and Ca^{2+} crosstalk caused by DJ-1 ablation compromises the stability of all three complex components [27]. However, the exact mechanism of abnormal MAMs in PD progression needs thorough exploration. Current study has revealed that EA potentially regulates the morphology and function of MAMs under pathological conditions [28]. On this basis, further investigation into whether EA alleviates PD by regulating MAMs and its potential mechanisms is essential. RNA sequencing (RNA-Seq) is an advanced technological method to locate and quantify the transcriptome by microarrays, thereby digitally measuring the presence and abundance of transcripts [29]. Evidence indicates that EA can regulate mRNA expression of differentially expressed genes (DEGs) in the mouse brain, influencing inflammation and related biolog-

ical processes [30–32]. However, the specific regulatory effects of EA at GV20 and GB34 on signaling pathways and genes in specific brain regions remain unclear.

This study hypothesizes that EA improves mitochondrial function by acting on MAMS, thereby alleviating dopaminergic neuronal degeneration and slowing the progression of PD. To test this hypothesis, transcriptome analysis of mouse brain tissue was employed to identify MAM-related pathways and key genes regulated by EA. Subsequently, the transcriptomic results were validated using real-time fluorescence quantitative polymerase chain reaction (RT-qPCR) to comprehensively clarify the potential therapeutic mechanisms of EA for PD.

2. Materials and Methods

2.1 Animal and Group Allocation

Male mice have more consistent physiological and metabolic responses, which helps reduce variability in experimental results [33]. C57BL/6 male mice were used to control for sex variables and improve the consistency and comparability of results. As effect sizes and standard deviations were not readily available directly from the existing literature and were difficult to estimate, the “resource equation method” was used to determine sample sizes [34,35]. This study was approved by the Experimental Animal Ethics Committee of Southern Medical University (Approval No. L2021119). Eighty-five eight-week-old male C57BL/6 mice (20–22 g) from Southern Medical University’s Animal Center (License No. SYXK[Yue]2021-0041) were acclimated for one week in a controlled environment (22 ± 2 °C, 12-hour light-dark cycle) with food and water *ad libitum*. To assess EA’s effect on MPTP-induced PD, mice were randomized into control ($n = 11$) and treatment ($n = 44$) groups. Treatment group mice were injected intraperitoneally with MPTP (30 mg/kg, Sigma-Aldrich, St Louis, MO, USA, dissolved in normal saline) once daily for seven consecutive days, while controls were administered equal volumes of saline (i.p.) [36]. The mice in the treatment group were then randomly and equally assigned to the MPTP, EA, drug and sham EA groups and received the corresponding treatments. Following behavioral analysis, mice were deeply anesthetized with 5% isoflurane (No. R510-22-10, RWD Life Science, Shenzhen, China) at a flow rate of 0.8 L/min and decapitated, after which brain tissues were collected for immunohistochemical, Western blot (WB) and transmission electron microscopy (TEM) assessments.

To further investigate EA’s influence on MAMs in the SN, mice were randomly divided into three groups (10 mice/group): control, MPTP and EA groups. Treatment and intervention were consistent with prior protocol, mice were then euthanized and the brain tissues were analyzed by WB, immunofluorescence, transcriptome analysis and RT-qPCR. The procedure is given in Fig. 1A.

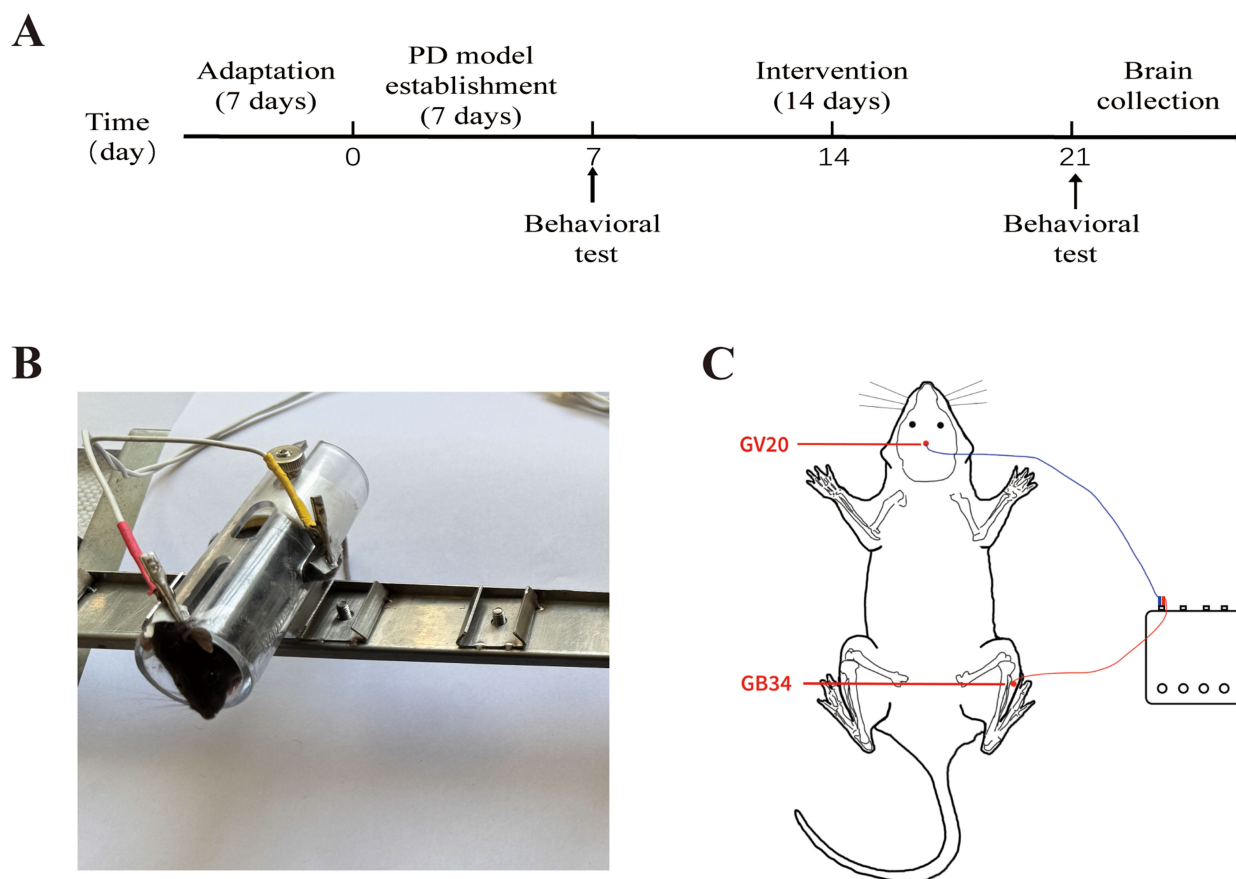


Fig. 1. Time axis of experimental procedures and positioning of acupoints. (A) Timeline outlining the experimental phases, including adaptation, PD model establishment, intervention, and brain collection, with behavioral tests scheduled at key time-points. (B) Photograph showing the setup of a mouse undergoing electroacupuncture treatment. (C) Schematic diagram depicting the selected electroacupuncture acupoints in a mouse: GV20 (middle of the parietal bone) and GB34 (lateral calf, in the depression below the anterior aspect of the fibular head). PD, Parkinson's disease; GV20, governing vessel 20; GB34, gallbladder meridian 34.

2.2 EA and Sham EA Procedure

EA treatment was conducted at the GV20 (middle of the parietal bone) and GB34 (lateral calf, in the depression below the anterior aspect of the fibular head) acupoints for 20 minutes daily following the induction of MPTP (Fig. 1B,C). GB34 on both sides was alternated daily. Acupuncture needles (0.16 mm × 5 mm; Suzhou Global Acupuncture Medical Equipment Co., Ltd., Suzhou, China) were inserted three mm deep at GV20 and unilateral GB34. The needles were then connected to electrodes delivering sparse-dense waves (5/100 Hz, 1 mA). Sham EA involved needle insertion at the same points without electrical stimulation. The entire treatment lasted 14 days [37].

2.3 Drug Administration

The drug group received levodopa (D9628, Sigma-Aldrich, dissolved in normal saline) and benserazide (B7283, Sigma-Aldrich, dissolved in normal saline) via intraperitoneal injection at a dose of 20 mg/kg and 5 mg/kg, respectively, once daily for 14 consecutive days.

2.4 Behavioral Tests

2.4.1 Pole Test

Before the experiment, animals were acclimatized for 12 hours, after which various behavioral tests were conducted, with an inter-test interval of one hour. Mice were placed on a wooden ball atop the pole-climbing apparatus (diameter 8 mm, height 50 cm). Timing started following stabilization. Key points: (T1) Center of mass crosses ball-pole junction, (T2) Reaches pole midpoint, (T3) Forelimbs touch ground. Scoring for each stage of the pole climbing test was determined based on the duration: three points awarded for 1–3 s, two points for 3–6 s and one point for exceeding 6 s or inability to maintain grip on the apparatus [38]. The entire test was repeated three times and mean values were calculated.

2.4.2 Rotarod Test

The Rotarod fatigue tester (JB-6C, Huai Bei 900 Electronic Technology Co., Ltd., Huaibei, Anhui, China) was set with parameters: Initial speed of four rpm, final speed 40 rpm, accelerated uniformly over five minutes [39]. Mice

were placed on the Rotarod with their heads facing inward. The acceleration program of the Rotarod was initiated and an infrared detection device with software was used to record the latency time from the start to the fall of the mouse (each mouse was tested three times and the average value was taken).

2.4.3 Wire Hanging Test

A custom wooden frame (length 50 cm, height 39 cm) with platforms at either end and a center steel wire (length 50 cm, diameter approximately 2 mm) supported the mouse's limbs for a 30 s test. Scoring: Falling 0, both forelimbs gripping 1, all four limbs gripping 2, wrapping tail and limbs 3, attempting to climb but failing 4, successful climb 5. Each mouse was tested three times, averaging scores. Tests were separated by 20 minutes to reduce fatigue [40].

2.4.4 Open Field Test

The apparatus (black plastic 40 × 40 cm) was divided into central (25% of total area) and peripheral zones. Mice were placed in the apparatus for five minutes under dim light. Total distance, average speed and trajectory were recorded and analyzed by the smart software (version 3.0; Panlab, S.L.U., Harvard Apparatus, Barcelona, Spain) [41].

2.5 Western Blot

Bilateral SN of four mice in each group were homogenized in lysis buffer prepared with a protein extraction kit (KGB5303-100, Nanjing KeyGen Biotech Co., Ltd., Nanjing, Jiangsu, China), followed by centrifugation and collection of supernatant. Protein concentration was measured using a Bicinchoninic Acid Protein Assay Kit (P0009, Shanghai Beyotime Biological Co., Ltd., Shanghai, China). Total lysates were denatured in sodium dodecyl sulphate-polyacrylamide gel electrophoresis (SDS-PAGE) sample loading buffer (NA0007, Beijing Leagene Bio-Technology Co., Ltd., Beijing, China) at 95 °C for eight minutes. 20 µg of protein were separated on 6%–12.5% SDS-PAGE gel and transferred onto a polyvinylidene fluoride (PVDF) membrane (ISEQ00010, Millipore, Bedford, MA, USA). After blocking with 5% nonfat milk in Tris-buffered saline with 0.05% Tween 20 for two hours at room temperature, the membranes were incubated overnight at 4 °C with the following primary antibodies: anti-IP3R (1:200; Santa Cruz Biotechnology, Santa Cruz, CA, USA; sc-377518), anti-Mfn2 (1:10,000; Proteintech, Wuhan, Hubei, China; 12186-1-AP), anti-VAPB (1:6000; Proteintech, 14477-1-AP), anti-TH (1:5000; Proteintech, 25859-1-AP), anti- α -syn (1:5000; Proteintech, 10842-1-AP) and anti-GAPDH (1:2000, Proteintech, 10494-1-AP). The following day, the PVDF membranes were washed and incubated with HRP-conjugated Affinipure Goat Anti-Rabbit IgG (H + L) (1:40,000; Proteintech, SA00001-2) for one hour at room temperature. After washing, immunoblot detection was

performed using an enhanced chemiluminescence Western blotting detection kit (WBKLS0500, Millipore, Bedford, MA, USA). Densitometry analysis was performed with ImageJ software (version 2.0.0, Rawak Software Inc., Stuttgart, Germany).

2.6 Immunohistochemistry

One hemisphere was separated and immersed in 4% paraformaldehyde for 24 hours, paraffin-embedded and sectioned into 6-µm-thick slices. Immunohistochemistry was performed following kit instructions (PV-9000, Zhongshan Golden Bridge Biotechnology Co., Ltd., Beijing, China). Brain sections underwent xylene deparaffinization and ethanol solutions (from 100% to 75%) and were washed with phosphate-buffered saline (PBS). Antigen retrieval was performed by boiling sections in Tris-EDTA buffer (pH 9.0) in a microwave oven for 15 minutes. Endogenous peroxidase blocking reagent was added dropwise to each section and incubated for 10 minutes at room temperature. After washing with PBS, the sections were incubated with the primary antibodies: anti-tyrosine hydroxylase (TH) (1:5000; Proteintech, 25859-1-AP) and anti- α -syn (1:500; Proteintech, 10842-1-AP) overnight at 4 °C. The next day, an appropriate amount of secondary antibody enhancement solution was added and incubated at 37 °C for 20 minutes. After washing with PBS, the sections were incubated with a biotinylated goat anti-mouse/rabbit IgG polymer at 37 °C for 20 minutes. Finally, the sections were incubated with the DAB substrate kit (ZLI-9018, Zhongshan Golden Bridge Biotechnology Co., Ltd., Beijing, China) at room temperature for five minutes and counterstained with hematoxylin (DH0006, Beijing Leagene Bio-Technology Co., Ltd., Beijing, China) and Nissl staining (DK0022100, Beijing Solaibao Technology Co., Ltd., Beijing, China). Images were captured using a pathology slide scanner (KF-PRO-005-EX, Ningbo Jiangfeng Biological Information Technology Co., Ningbo, Zhejiang, China).

2.7 Immunofluorescence

Brains were perfused transcardially with 4% paraformaldehyde, fixing the entire organ. Post-fixation, hemispheres were separated, and one hemisphere was processed for immunofluorescence and sliced into 20-micron frozen sections. These sections were immersed in Frozen Sections Antigen Repair Agent (P0090, Shanghai Beyotime Biological Co., Ltd.), followed by three washes and incubation in 0.3% Triton X-100 (T9284, Sigma-Aldrich) for 30 minutes. After washing with PBS, sections were blocked with PBS solution containing 5% goat serum (16210064, Gibco, New York, NY, USA) for 30 minutes. Sections were then incubated with primary antibodies overnight at 4 °C: anti-translocase of outer mitochondrial membrane 20 (TOM20) (1:500; Santa Cruz Biotechnology, Santa Cruz, CA, USA; SC-17764) and

Table 1. Primer sequences of the targeted genes in mice.

Targeted genes	Forward and reverse primers
Myocilin (<i>Myoc</i>)	CAGGGAAGTCTCTCAGTGGGAATT (F) GGTCTCTCATCCACACTCCATAC (R)
Proprotein Convertase Subtilisin/Kexin Type 9 (<i>Pcsk9</i>)	TATGACCTCTTCCCTGGCTTCTT (F) GGATAATTCGCTCCAGGTTCCAT (R)
Fibronectin 1 (<i>Fn1</i>)	TGAGCGAGGAGGGAGATGAA (F) TAGGTGCCTGGGGTCTACTC (R)
Cubilin (<i>Cubn</i>)	TCTGGCATCTTGGAGAGCATAAA (F) TTTCTCCACAGTAGCGTCCTATC (R)
Integrin Alpha 5 (<i>Itga5</i>)	GCTGGACTGTGGTGAAGACAATA (F) AATGTCAGGTTTCAGTGCCTTCTT (R)
Dopamine Receptor D1 (<i>Drd1</i>)	AGGTTGAGCAGGACATACGC (F) TTGCTTCTGGGCAATCCTGT (R)
Adenosine A2a Receptor (<i>Adora2a</i>)	TCACGCAGAGTTCCATCTTCAG (F) AGGTCTTTGTGGAGTTCTCATCTT (R)
Cluster of Differentiation 4 (<i>Cd4</i>)	CCTGACCTTGGATAGCAACTCTAA (F) CGCTGACTCTCCCTCACTCTTAT (R)
Glyceraldehyde-3-Phosphate Dehydrogenase (<i>GAPDH</i>)	CATCACTGCCACCCAGAAGACTG (F) ATGCCAGTGAGCTTCCCGTTCAG (R)

anti-calreticulin (1:500; Proteintech,10292-1-AP). After washing,slices were dark incubated for two hours with goat anti-rabbit Alexa Fluor 488-conjugate IgG (1:500; Abcam, Cambridge, UK; ab150077) and goat anti-mouse Alexa Fluor 647-conjugate IgG (1:500; Abcam, ab150115). Finally, slices were mounted using Fluoroshield with 4',6-diamidino-2-phenylindole (DAPI) (F6057, Sigma-Aldrich) and imaged using a Leica BX53 fluorescent microscope.

2.8 Transmission Electron Microscopy

The SN tissue on one side of three mice in each group was taken as a sample and fixed in 2.5% glutaraldehyde overnight. Samples were then rinsed in buffer, post-fixed in 1.0% osmium tetroxide for one hour, rinsed again, and dehydrated through graded ethanol series. After resin embedding, the samples were made into ultrathin sections. These sections were viewed on a TEM (H-7500, Hitachi, Tokyo, Japan).

2.9 Transcriptome Analysis

The SN tissue from the remaining side of three mice in each group was used for transcriptomic analysis. Shanghai Majorbio Bio-pharm Biotechnology Co., Ltd. (Shanghai, China) performed all transcriptomic procedures—including RNA purification, reverse transcription, library preparation (TruSeqTM RNA Kit, Illumina; 1 µg total RNA), and Illumina platform sequencing—according to the Illumina's instructions (San Diego, CA, USA). Principal component analysis of gene expression profiles was performed using the platform (<https://www.majorbio.com>). The DEseq2 algorithm based on the platform was used to identify DEGs among the control, MPTP and EA groups. The fold change

threshold was set at $|\log_2 \text{fold change}| \geq 1.5$ and the adjusted p -value was set to <0.05 . A Venn diagram was used to identify the key DEGs related to the effect of EA, focusing on those that showed expression levels closer to the controls. The expression levels of DEGs were visualized with a heatmap based on the platform. The gene sets related to MAMs were downloaded and compared with DEGs on the platform. Furthermore, functional enrichment analysis including Gene Ontology (GO), Kyoto Encyclopedia of Genes and Genomes (KEGG) and Reactome was conducted to identify significantly enriched DEGs with a Bonferroni-corrected p -value ≤ 0.05 , compared to that of the whole-transcriptome.

2.10 RT-qPCR

Total RNA from the SN of four mice in each group was extracted using TRIzol reagent (15596026CN, Invitrogen, Carlsbad, CA, USA). A BioTek spectrophotometer was used to detect the concentration and purity of RNA, which was then diluted in a proportion appropriate to make a final concentration of 1000 ng/µL. The Evo M-MLV Reverse Transcription Kit (AG11705, Accurate Biotechnology, Changsha, Hunan, China) was used to synthesize cDNA by reverse transcription of total RNA. The target gene expression levels were determined with a synergetic binding reagent (SYBR) RT-PCR kit (AG11739, Accurate Biotechnology, Changsha, Hunan, China). RT-qPCR was performed using a Roche LightCycler 96. Primers were procured from TSINGKE (Beijing, China) and the sequences are shown in Table 1. *GAPDH* was considered as the housekeeping gene to normalize the expression levels of targeted genes, three parallel holes were set for every

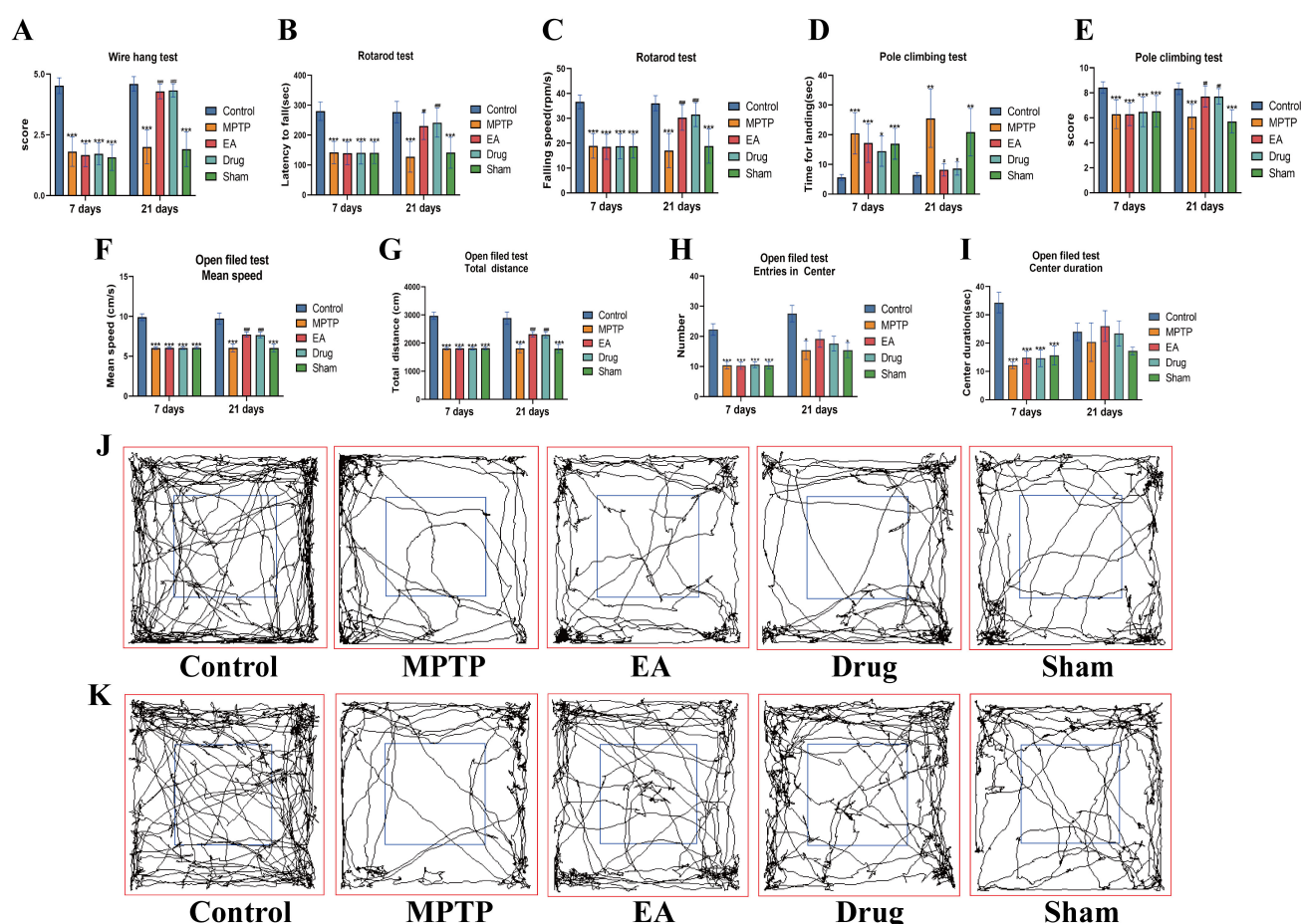


Fig. 2. Behavioral analysis. (A) Time to landing in the pole climbing test (Day 7 $F = 7.645$, $p < 0.001$; Day 21 $F = 15.396$, $p < 0.001$). (B) Score in pole climbing test (E, Day 7 $F = 4.106$, $p = 0.009$; Day 21 $F = 14.49$, $p < 0.001$). (C) Latency to fall in the rotarod test (Day 7 $F = 21.235$, $p < 0.001$; Day 21 $F = 13.74$, $p < 0.001$). (D) Falling speed in the rotarod test (Day 7 $F = 21.262$, $p < 0.001$; Day 21 $F = 15.955$, $p < 0.001$). (E) Score in the wire hang test (Day 7 $F = 47.845$, $p < 0.001$; Day 21 $F = 50.77$, $p < 0.001$). (F–I) Parameters measured in open field test (Mean speed, Day 7 $F = 359.523$, $p < 0.001$; Day 21 $F = 66.39$, $p < 0.001$; Total distance, Day 7 $F = 360.298$, $p < 0.001$; Day 21 $F = 60.63$, $p < 0.001$; Entries in Center, Day 7 $F = 15.545$, $p < 0.001$; Day 21 $F = 3.401$, $p = 0.021$; Center duration, Day 7 $F = 10.309$, $p < 0.001$; Day 21 $F = 1.533$, no significant difference). (J) Representative track maps of each group in open field test Day 7. (K) Representative track maps of each group in open field test Day 21. Data were presented as mean \pm standard error of the mean. * $p < 0.05$, ** $p < 0.01$, *** $p < 0.001$ vs. Control; # $p < 0.05$, ## $p < 0.01$, ### $p < 0.001$ vs. MPTP; $n = 7$, one-way analysis of variance with Bonferroni *post hoc* test used. MPTP, 1-methyl-4-phenyl-1,2,3,6-tetrahydropyridine; EA, electroacupuncture.

sample and the relative expression of genes was analyzed according to the $2^{-\Delta\Delta C_t}$ method.

2.11 Statistical Analyses

To analyze data, the average of several groups of data was calculated and outliers with scores greater than 1.5 interquartile ranges from the first and third quartiles of the data distribution were eliminated. Additionally, after excluding outliers, to ensure consistency in the number of animals per group, an equal number of animals were randomly selected from each group for evaluation. Statistical analysis was conducted using GraphPad Prism 9.0 (GraphPad Software, Inc., San Diego, CA, USA). Data are reported as mean \pm standard error of the mean. Normally distributed data were compared using one-way analysis of variance

(ANOVA) followed by a Bonferroni multiple comparison test (variances equal) or the Dunnett T3 test (variances unequal) [42] with statistical significance assumed for $p < 0.05$. Non-normally distributed data were analyzed using the Kruskal-wallis test. Graphs were obtained from Graph-Pad Prism 9.0.

3. Results

3.1 Motor Dysfunction Improvements and Neuroprotective Effects of EA

To determine whether EA can increase motor function in the MPTP model, pole climbing, rotarod, wire hang and open field tests were performed. Following successful establishment of the PD mouse model on day seven, behavioral assessments revealed that MPTP-treated mice

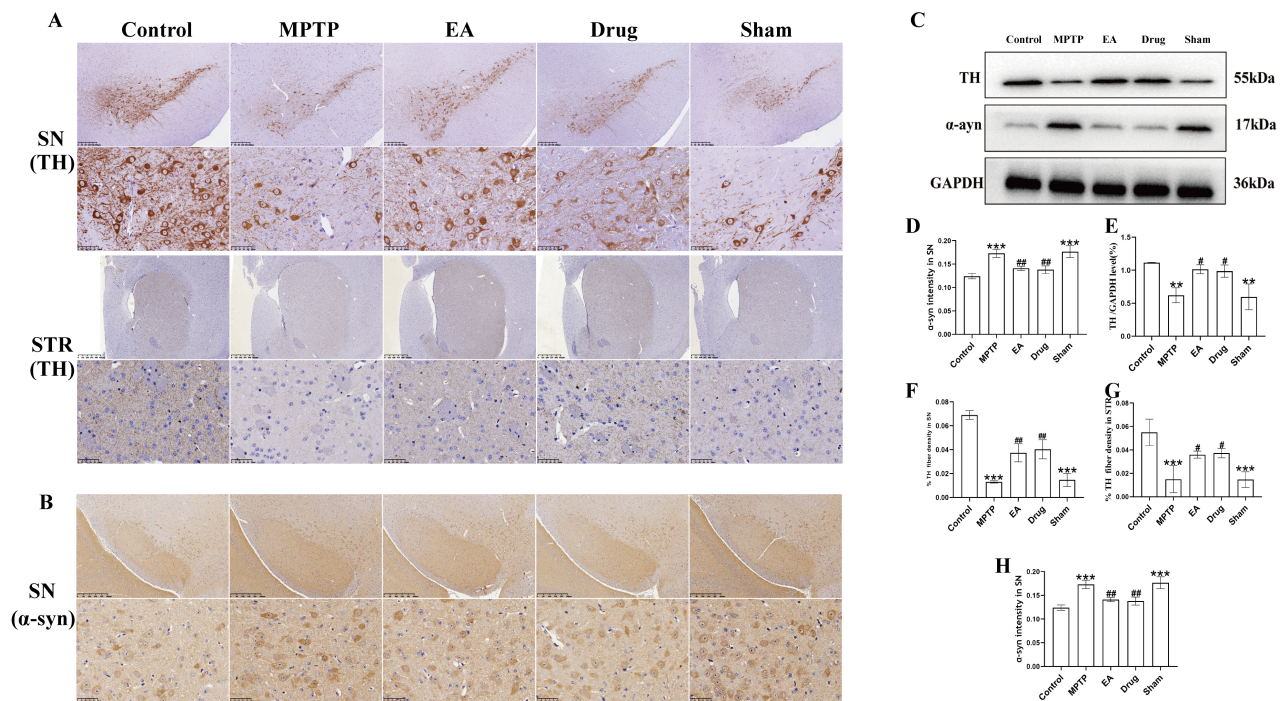


Fig. 3. EA ameliorated neuropathological alterations produced by MPTP in PD mice. (A) Representative immunohistochemistry analysis of TH for SN and STR. Magnifications of $\times 40$ were taken. Top row enlarges the original image by $\times 5$ (scale bar: SN 200 μm ; STR 625 μm), the bottom row enlarges the original image by $\times 40$ (scale bar: SN 50 μm ; STR 50 μm). (B) Representative immunohistochemistry analysis of α -syn, magnification as above (scale bar: top row 400 μm ; the bottom row 50 μm). (C) Western blot of TH, α -syn and GAPDH expression in the SN. (D,E) Quantitative analysis of Western blots for α -syn (D, $F = 8.188$, $p = 0.003$) and TH (E, $F = 13.43$, $p = 0.005$). (F,G) Optical density of TH⁺ fiber immunoreactivity in SN (F, $F = 47.15$, $p < 0.001$) and STR ((G), $F = 22.25$, $p < 0.001$). (H) Quantitative results of α -syn-positive aggregates ($F = 13.22$, $p = 0.0005$). SN, substantia nigra; STR, striatum; TH, tyrosine hydroxylase; α -syn, α -synuclein; Data presented as mean \pm standard error of the mean. ** $p < 0.01$, *** $p < 0.001$ vs. Control; # $p < 0.05$, ## $p < 0.01$ vs. MPTP; $n = 3$, one-way analysis of variance with Bonferroni *post hoc* test was used.

exhibited significant motor impairments across all tests (Fig. 2), confirming the successful replication of Parkinsonian motor dysfunction characteristics and providing a reliable model for subsequent intervention studies. Moreover, there were no statistical differences between the treatment groups, which excludes the interference of factors on the results that may have existed prior to the implementation of the intervention, thus avoiding false-positive results post-intervention. After 14 days of counterpart interventions, one-way ANOVA showed significant differences among the groups in the behavioral tests. In the pole climbing test, the total landing time of the MPTP group mice was significantly prolonged ($p < 0.001$ vs. control, Fig. 2A). The scores of the MPTP group were significantly reduced in the pole climbing and wire hang tests ($p < 0.001$ vs. control, as shown in Fig. 2B,E). The MPTP group also exhibited a markedly diminished latency to fall and a lower falling speed in the rotarod test ($p < 0.001$ vs. control, as shown in Fig. 2C,D). Furthermore, the total distance and average speed of mice in the MPTP group in the open field test were also found to be significantly reduced ($p < 0.001$ vs. control, Fig. 2F,G). Representative track maps

for each group demonstrated the same trend (Fig. 2J,K). Meanwhile, mice in the MPTP group exhibited a significant reduction in both the time spent in the central zone and the number of entries into the central zone. These findings suggest that MPTP-treated PD mice display anxiety-like behaviors, characterized by a marked decrease in exploratory activity ($p < 0.001$ vs. control, Fig. 2H,I). In contrast, the EA and drug groups demonstrated functional recovery as evidenced by their performance in the behavioral tests, while the sham EA group showed no recovery (Fig. 2). These results clearly demonstrate that EA exhibits significant effects in promoting MPTP-induced motor function recovery in Parkinsonian mice. A reduction in tyrosine hydroxylase (TH) activity leads to diminished DA production, which impairs neuronal function and may contribute to the pathogenesis of PD [43], while α -syn is a pathological marker of PD [44]. The neuroprotective effect of EA on MPTP-induced neuronal death was evaluated by measuring TH levels in STR and SN and α -syn level in SN. As depicted in Fig. 3, a comparison of the optical density of TH-positive cells in the SN revealed a significant reduction in the MPTP and sham EA groups relative to con-

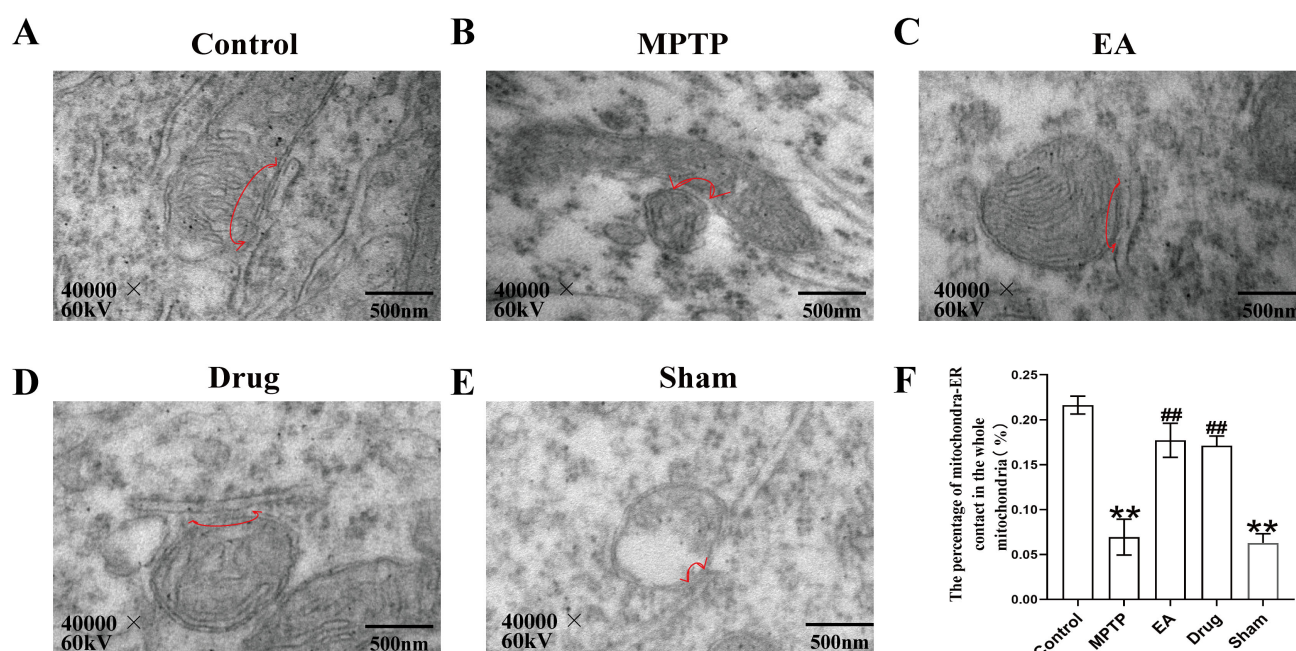


Fig. 4. Results of endoplasmic reticulum membranes in the SN in each group of mice were observed under transmission electron microscope. (A–E) Representative transmission electron micrographs for each group, the arrowheads with loops show regions of association. (F) The percentage of the mitochondria surface closely apposed to endoplasmic reticulum (defined as ≤ 30 nm proximity) in the whole mitochondria of different groups ($F = 21.41$, $p = 0.0019$). Data were presented as mean \pm standard error of the mean. ** $p < 0.01$ vs. Control; ## $p < 0.01$ vs. MPTP; $n = 3$, one-way analysis of variance with Bonferroni *post hoc* test used. Magnification: 40,000 \times , scale bar: 500 nm.

trols ($p < 0.001$, Fig. 3A,F); however, the optical density was markedly higher in the EA and drug groups than in the MPTP and sham EA groups ($p < 0.01$, $p < 0.001$, respectively). A comparable trend was observed in the optical density of the STR (Fig. 3A,G). Furthermore, α -syn levels were elevated in the MPTP and sham EA groups ($p < 0.001$ vs. control, Fig. 3B,H), whereas EA and drug treatment resulted in a significant reduction in α -syn levels ($p < 0.001$ vs. MPTP group). The WB results offer further corroboration of the morphological findings (Fig. 3C–E, the original WB figures for Fig. 3C are provided in the **Supplementary Materials**). Based on the results of IHC and WB experiments, it can be concluded that EA effectively alleviates the accumulation phenomenon of α -syn in the SN.

3.2 EA Improved the Loose Structure of MAMs in the SN of PD Mice

MAMs in the SN were observed through TEM. As shown in Fig. 4, compared with controls MAMs in the MPTP and sham groups were loose, with significant distance between mitochondria and ER, reducing the percentage of mitochondrial-ER contact in the whole mitochondria ($p < 0.01$ vs. control, Fig. 4F). In contrast, the MAMs in the EA and drug groups were tighter ($p < 0.01$ vs. MPTP group). To further explore the specific effects of EA intervention on MAMs, immunofluorescence and WB were performed on control, MPTP and EA groups. The double-labelling immunofluorescence technique was employed ac-

cording to [45], using translocase of outer mitochondrial membrane 20 (TOM20) and calreticulin (CRT), to observe and analyze the level of intracellular mitochondrial-ER colocalization. Results showed that the mitochondrial-ER colocalization coefficient decreased in the MPTP group when compared to control, but increased in the EA group compared to the MPTP (Fig. 5A,C). IP3R, Mfn2 and VAPB are essential components of highly dynamic protein complexes and the collection of functional regulatory proteins that make up MAMs. Once the expression of these proteins is reduced, it leads to the structure of MAMs becoming loose and triggers their functional disorder [46,47]. WB results showed IP3R, Mfn2 and VAPB protein levels in SN tissue of the MPTP group decreased (Fig. 5B, $p < 0.05$, $p < 0.05$ vs. control, respectively; the original WB figures for Fig. 5B are provided in the **Supplementary Materials**). In the EA group, these protein levels significantly increased ($p < 0.01$, $p < 0.05$, $p < 0.01$ vs. MPTP group, respectively, Fig. 5D–F). These results strongly suggest that EA in PD significantly improves the morphology and function of MAMs in SN neurons.

3.3 EA Altered Genome Wide Gene Expression

To explore EA's mechanism in PD, gene expression profiling was completed for different groups. A volcano map revealed 1008 DEGs in the MPTP vs. control (658 up, 350 down). Between the MPTP and EA groups, 869

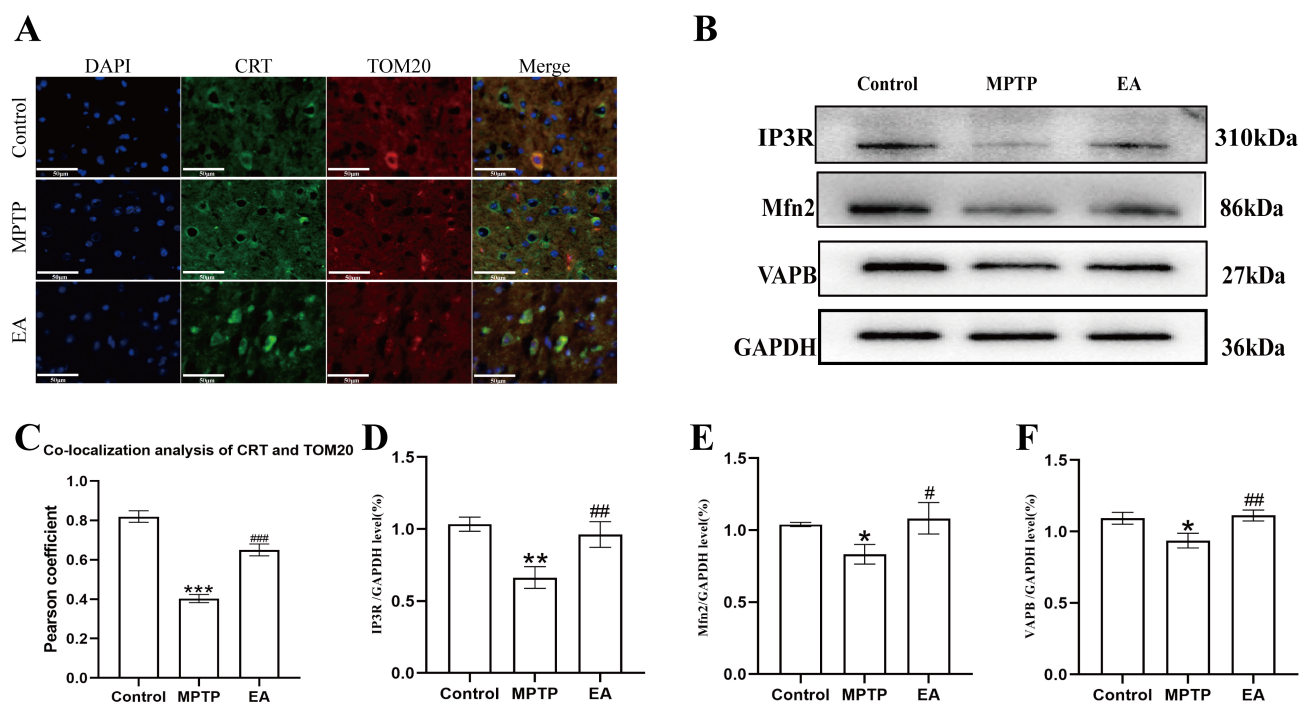


Fig. 5. Effect of EA on MPTP-induced changes of MAMs in PD mice. (A) Co-localization of ER and mitochondria in each group of substantia nigra neurons detected by immunofluorescence. DAPI marks the nucleus blue. TOM20 stains the mitochondria red. CRT marks the endoplasmic reticulum, shown as green. The overlapping area of TOM20 and CRT represents the MAMs (magnification, $\times 200$). (B) Western blots of IP3R, Mfn2, VAPB and GAPDH expression in the SN. (C) Quantified colocalization of CRT with TOM20 assessed by the Pearson coefficient ($F = 176.881$, $p < 0.001$). (D–F) Quantitative results of IP3R ($F = 60.58$, $p < 0.001$), Mfn2 ($F = 9.558$, $p = 0.013$), VAPB ($F = 14.38$, $p = 0.005$). DAPI, 4',6-Diamidino-2'-phenylindole; TOM20, translocase of outer mitochondrial membrane 20; CRT, calreticulin; IP3R, inositol1,4,5-trisphosphate receptors; Mfn2, mitofusin 2; VAPB, vesicle associated membrane protein associated protein B; ER, endoplasmic reticulum. Data given as mean \pm standard error of the mean. * $p < 0.05$, ** $p < 0.01$, *** $p < 0.001$ vs. Control; # $p < 0.05$, ## $p < 0.01$, ### $p < 0.001$ vs. MPTP; $n = 3$, one-way analysis of variance with Bonferroni *post hoc* test used.

DEGs were identified (364 up, 505 down). Heat maps visualized expression patterns of up-regulated and down-regulated genes for the control, MPTP and EA groups. As Fig. 6A shows, red and blue colors respectively illustrate higher and lower expression of genes. DEGs overlaps were then analyzed with Venn diagrams (Fig. 6B). EA downregulated 231 of the 658 up-regulated DEGs and upregulated 98 of the 350 down-regulated DEGs in the MPTP group. The 329 DEGs may be key EA targets against PD, as shown in the heat map (Fig. 6C).

To investigate the function of the DEGs, GO classification, KEGG and Reactome annotations, analysis and enrichment analyses were performed. Following the GO database, three different ontologies were used to annotate the genes, including biological process (BP), cellular component (CC) and molecular function (MF). In GO BP terms, the DEGs were mostly enriched in catalytic activity and binding. The DEGs were mostly enriched in cell and membrane part categories according to their CC classification. MF DEGs were mostly enriched in cellular processes and biological regulation (Fig. 6D). To identify key pathways

modulated by EA in PD, we analyzed DEGs via KEGG pathway enrichment. KEGG pathway analysis revealed EA modulation of the first three pathways: neuroactive ligand-receptor interactions, morphine addiction and dopaminergic synapses (Fig. 6E). Reactome analysis showed EA modulation of signaling, G protein-coupled receptor (GPCR) signaling and downstream GPCR signaling (Fig. 6F).

3.4 Transcriptomic Analysis of MAMs-Related Genes Regulated by EA

To explore the mechanism of EA regulation of MAMs in depth, a Venn diagram analysis was performed of 329 genes potentially regulated by EA with genes that are known to be associated with the regulation of MAMs in the GO database. 32 candidate genes most likely to be key players in the regulation of MAMs function and activity were screened by electroacupuncture (Fig. 7A). To visualize the specific changes of these genes in different experimental groups, heat maps were created to clearly show their expression differences (Fig. 7B). These DEGs were analyzed for GO and KEGG pathway enrichment to further reveal the mechanism of EA regulation of MAMs. The MF were

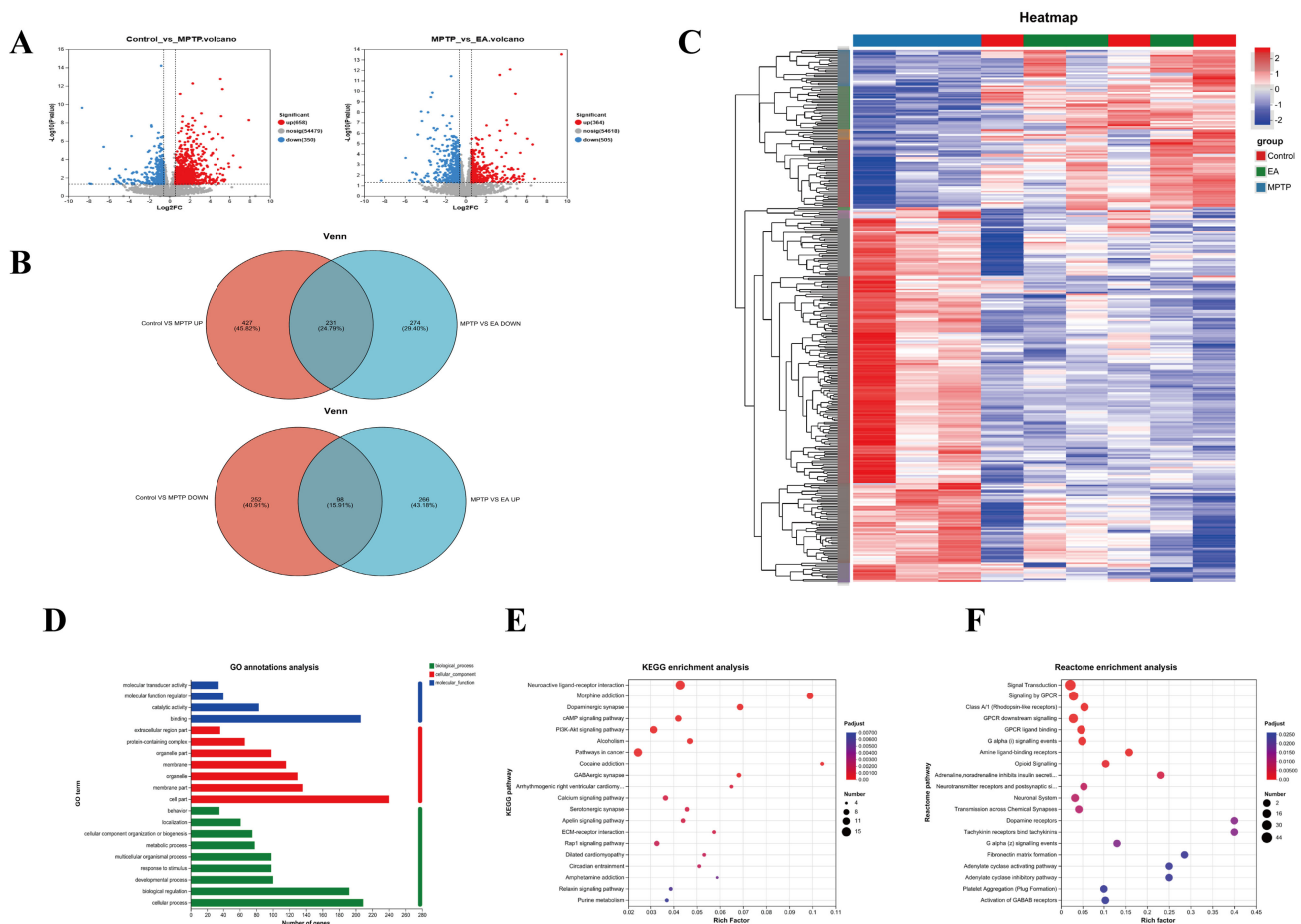


Fig. 6. Analysis of mice transcriptome samples. (A) Volcano plot for ($|\log_2\text{FC}| > 1.5, p < 0.05$). (B) Venn diagram of differentially expressed genes (DEGs). (C) Heat map of DEGs. (D) Gene Ontology (GO) functional annotation classification of DEGs. (E,F) Kyoto Encyclopedia of Genes and Genomes (KEGG) and Reactome enrichment analysis of DEGs.

mainly enriched in biological regulation, cellular process, and response to stimulus; the CC was enriched in cell part, membrane part and membrane, the BP was primarily enriched in binding, catalytic activity and transporter activity (Fig. 7D). Pathway analysis showed that the MAMs pathways were inhibited, such as calcium signaling pathway, cAMP signaling pathway and ECM-receptor interaction pathway (Fig. 7E). A protein-protein interaction network was constructed using the STRING database (Fig. 7C). These findings provide further evidence that fibronectin-1 (*Fnl*) is strongly associated with MAMs. The results indicated that EA may influence MAMs by enhancing the expression of *Fnl*, thereby providing a potential treatment for PD.

3.5 Validation of the DEGs Using RT-qPCR

To validate RNA-Seq data reliability, we examined eight DEGs: adenosine a2a receptor (*Adora2a*), cluster of differentiation 4 (*Cd4*), cubilin (*Cubn*), dopamine receptor d1 (*Drd1*), fibronectin 1 (*Fnl*), integrin alpha 5 (*Itga5*), myocilin (*Myoc*) and proprotein convertase subtilisin/kexin type 9 (*Pcsk9*). Their expression trends (Fig. 8) matched

RNA-Seq profiles. Three genes (*Cubn*, *Fnl* and *Myoc*) were downregulated in the MPTP group (Fig. 8C,E,G) but upregulated by EA. Conversely, five genes (*Adora2a*, *Cd4*, *Drd1*, *Itga5* and *Pcsk9*) were upregulated in the MPTP group but downregulated by EA (Fig. 8A,B,D,F,H).

4. Discussion

A PD model induced by MPTP compounds is one of the most commonly used disease models for PD [48]. After seven days of MPTP injection, all experimental mice except the control showed significant impairment in wire hanging, rotarod, climbing and open field tests, confirming successful model establishment. In contrast, the EA and drug groups exhibited significant recovery, while the sham EA group did not. These behavioral results suggest that EA at GV20 and GB34 effectively enhances motor coordination, balance, limb strength and overall motor function in mice with PD with effects comparable to those of positive drugs.

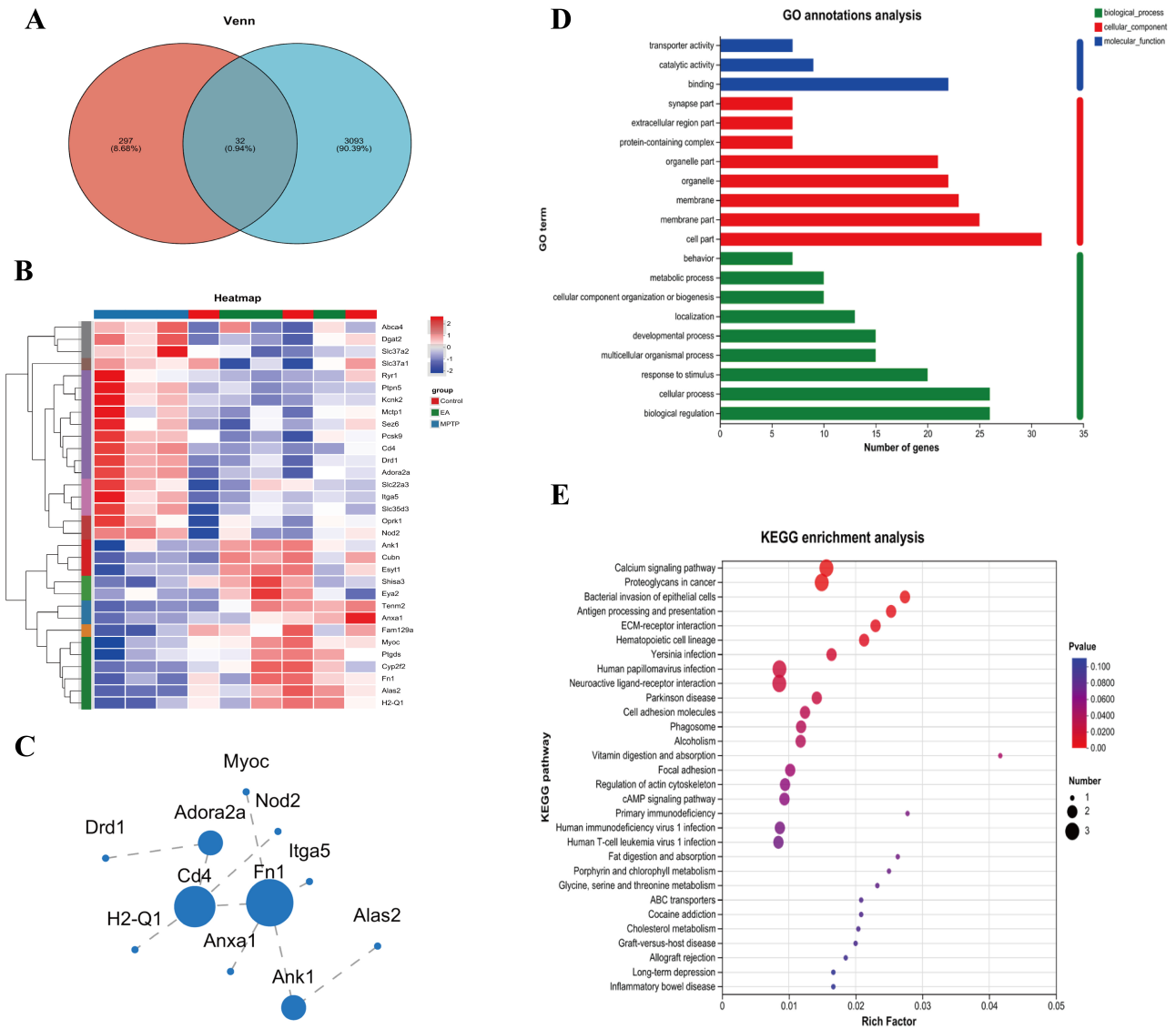


Fig. 7. MAMs-related transcriptomic analysis. DEGs: (A) Venn diagram; (B) Heat map; (C) Protein-protein interaction analysis; (D) GO functional annotation classification; (E) KEGG enrichment analysis.

Given that motor function recovery likely reflects neuronal protection, next investigation was dopaminergic neuron integrity. TH plays a key role in regulating DA biosynthesis and TH-positive neurons may represent dopaminergic neurons [49]. According to the results of immunohistochemistry (IHC) and WB experiments, the optical density of TH in the STR and SN, which had been reduced in the MPTP group, was notably increased following EA. Meanwhile, the accumulation of pathological protein α -syn in the SN was reduced after EA, confirming that EA has a protective effect on dopaminergic neurons and potentially removes the pathological protein α -syn.

To explore the mechanism of EA, its effect on MAMs was examined. TEM showed loose mitochondrial-ER coupling and reduced coupling areas in the MPTP group, which were enhanced by EA. TOM20 and CRT immunofluorescence co-staining results further supported these findings,

indicating that EA may enhance neuroprotection by promoting mitochondrial-ER coupling. This may be linked to the recovery of the expression of MAMs-related proteins such as IP3R, Mfn2 and VAPB. WB results showed that the expression levels of IP3R, Mfn2 and VAPB showed a decreasing trend in the MPTP-induced mouse model of PD and EA was shown to be effective in ameliorating this pathology. These proteins play pivotal roles in MAMs. Mfn2, a regulator of mitochondrial fusion, not only establishes physical connections between the ER and mitochondria but also regulates Ca^{2+} transfer [50]. The absence of Mfn2 has been shown to reduce mitochondrial-ER connectivity and Ca^{2+} uptake [51]. IP3R facilitates the mitochondrial-ER coupling by forming complexes with glucose-regulated protein 75 kDa (GRP75) and voltage-dependent anion channel (VDAC), thereby enhancing mitochondrial Ca^{2+} uptake and ATP production [27]. Mean-

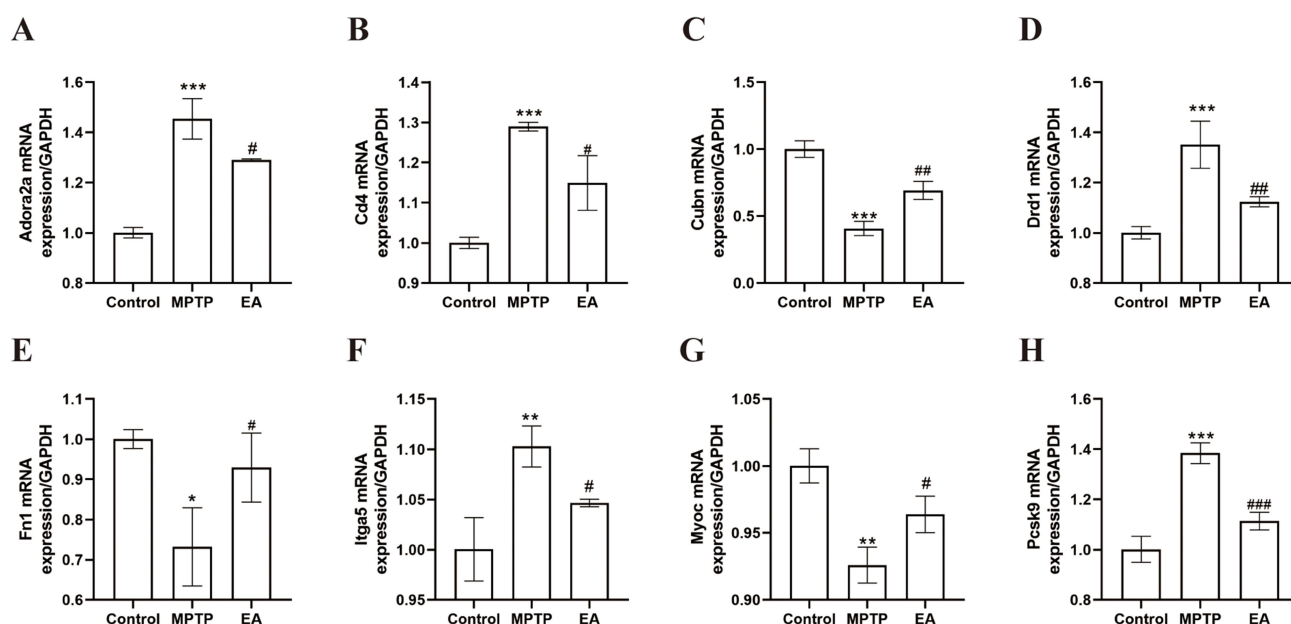


Fig. 8. Confirmation of RNA sequencing results by real-time fluorescence quantitative polymerase chain reaction (RT-qPCR). (A) *Adora2a* ($F = 68.08, p < 0.001$). (B) *Cd4* ($F = 38.03, p < 0.001$). (C) *Cubn* ($F = 69.89, p < 0.001$). (D) *Drd1* ($F = 29.08, p < 0.001$). (E) *Fn1* ($F = 9.999, p = 0.0012$). (F) *Itga5* ($F = 16.60, p = 0.0036$). (G) *Myoc* ($F = 23.53, p < 0.001$). (H) *Pcsk9* ($F = 62.25, p < 0.001$). Data were presented as mean \pm standard error of the mean. * $p < 0.05$, ** $p < 0.01$, *** $p < 0.001$ vs. Control; # $p < 0.05$, ## $p < 0.01$, ### $p < 0.001$ vs. MPTP; $n = 3$, one-way analysis of variance with Bonferroni *post hoc* test.

while, VAPB, in conjunction with phosphatase-interacting protein 51, regulates the transfer of Ca^{2+} between the ER and mitochondria and disruption of this interaction leads to the dissociation of MAMs and subsequent mitochondrial dysfunction [52]. Therefore, the restoration of these proteins by EA likely underpins the observed improvement in MAMs structure. Further mechanistic studies may focus on Ca^{2+} signaling and ATP synthesis in MAMs [53,54].

To further elucidate the molecular pathways involved in EA modulation of MAMs, RNA-Seq analysis showed significant regulation by EA in PD mice. When compared to controls, 1008 DEGs were identified in the MPTP group and EA altered 869 genes. Venn diagram analysis revealed reversal of 231 upregulated and 98 downregulated genes, suggesting key targets. Further analysis revealed that EA modulated 32 MAMs-related genes. GO analysis indicated involvement in biological regulation, cellular processes and response to stimuli, while KEGG pathway enrichment linked these genes to MAM-associated pathways, including calcium and cAMP signaling and extracellular matrix (ECM) interactions. EA reversed the suppression of these pathways in PD, suggesting a role in delaying PD progression. These results add another layer of support to the claim that EA, by modulating MAMs, improves calcium signaling, optimizes the intracellular environment and in turn, has a beneficial effect on PD. The RT-qPCR validation of *Adora2a*, *Cd4*, *Cubn*, *Drd1*, *Fn1*, *Itga5*, *Myoc* and *Pcsk9* exhibited concordance with the RNA-Seq data, providing further evidence of EA's modulatory impact.

Concurrently, through a comprehensive examination of the protein network interactions of DEGs, *Fn1* was identified as a core gene regulated by EA. Based on these findings, it is plausible to hypothesize that EA at GV20 and GB34 is likely to exert its therapeutic effect on PD by modulating the expression of *Fn1*, which in turn affects MAMs. *Fn1*, as a large glycoprotein, is a crucial component of the ECM and plays a key role in cell adhesion and migration processes [55]. *Fn1* is closely related to the ECM-receptor interaction signaling pathway involved in various cancer-related processes [56]. The present study observed a significant enrichment of *Fn1* in the ECM-receptor interaction pathway, providing evidence to support the hypothesis that EA may mediate this pathway through *Fn1*, thereby exerting its biological effects. Specifically, the interaction of *Fn1* with integrins activates Focal Adhesion Kinase (FAK) and Steroid receptor coactivator (Src) family kinases [57], thereby triggering a series of complex signaling cascades that potentially impact the structure and material exchange between the mitochondria and ER. In PD, decreased FAK levels may impair the autophagic response to ER stress, leading to its persistence and exacerbation. This aggravation may further lead to the loosening of the MAMs structure, which hinders the essential material exchange and signaling between the ER and mitochondria. This, in turn, disrupts cellular homeostasis and accelerates PD progression [58]. Furthermore, *Fn1* deficiency may negatively impact mitochondrial function by inhibiting the FAK/STAT3 pathway, resulting in mitochondrial dysfunction, loss of mem-

brane potential and increased reactive oxygen species production. This similarly affects the material exchange between mitochondria and the ER within MAMs [59]. Fnl also interacts with the PI3K-Akt pathway [60], which regulates Ca^{2+} exchange between the ER and mitochondria by modulating key proteins such as GRP75, IP3R and VDAC [61]. Previous study has shown that inhibiting the PI3K/Akt pathway leads to structural damage to MAMs [62]. Additionally, downregulation of the *Fnl* gene leads to decreased expression of Bcl-2 protein and increased expression of Bax protein [63]. Anti-apoptotic proteins such as Bcl-2 are typically located on the mitochondrial membrane, where they influence the function and stability of mitochondria [64]. This may indirectly affect the structure and function of MAMs. On the basis of such evidence, it is hypothesized here that EA may regulate the interaction between *Fnl* and integrins by up-regulating the expression or enhancing the activity of *Fnl*. This regulatory process subsequently affects the activation of FAK and Src family kinases and ultimately influences the structure and function of MAMs through related signaling pathways. Additionally, EA may indirectly modulate *Fnl*'s role in MAMs by regulating the FAK/STAT3 and PI3K-Akt pathways. Therefore, future studies should further explore the specific mechanisms by which EA therapies modulate the effects of *Fnl* on MAMs, providing new insights and approaches for advancing this field.

This study reveals a novel mechanism by which EA may exert its neuroprotective effects in ameliorating PD symptoms by enhancing MAMs structure and function, potentially through the restoration of key MAMs proteins (IP3R, Mfn2 and VAPB) and the modulation of critical pathways involving genes like *Fnl*. Future studies should further explore how EA can fulfill its potential in the treatment of PD by modulating these MAMs-related proteins and their mediated Ca^{2+} signaling and energy metabolism processes, with a specific focus on validating the Fnl-MAMs axis.

However, this study has several limitations. While RNA-Seq showed effects on multiple genes and pathways and identified Fnl as a key EA-regulated gene that influences MAMs, the specific underlying mechanisms require further validation. To further elucidate these mechanisms, it is planned to develop a CRISPR-dCas9 activation/repression system to specifically regulate *Fnl* expression in the SN pars compacta. This approach will be combined with AAV-mediated MAMs reporter viruses to dynamically dissect the functional axis of Fnl-MAMs. Additionally, the exploration of MAMs in the present study focused primarily on structure and protein composition, while the effects of Ca^{2+} dynamics (e.g., IP3R-GRP75-VDAC1 flux) and ATP production following changes in MAMs have not been studied in detail. Future research will employ live-cell imaging techniques to dynamically monitor Ca^{2+} oscillations and ATP production rates. Meanwhile, focus will be on the regulation of *Fnl* expression and ac-

tivity by EA therapy and its effect on Fnl-integrin interactions. The central goal is to elucidate how EA regulates *Fnl* binding to integrins at the molecular level and how this regulation further affects the structure and function of MAMs. There were some limitations in the experimental design of this study and the unfinished experimental elements included MAMs-associated immunofluorescence colocalization analyses, WB assays and transcriptomics analyses in the sham and drug groups, which may affect comprehensive assessment of the effects of EA and drug interventions on the structure and function of MAMs, as well as in-depth understanding of the regulatory mechanisms of related gene expression. The small sample size is a limitation of the current study, which may hinder a comprehensive assessment of the combined effects of EA in PD. Also, a focus on midbrain dopaminergic neurons may overlook changes in other brain regions. The inability to conduct long-term behavioral assessments also limits the generalizability of findings regarding the sustained impact of EA. Future studies should refine these experimental elements and incorporate multimodal imaging, larger samples and extended durations are required to clarify the comprehensive effects of EA in PD. Single-nucleus sequencing should be integrated with spatial transcriptomics to generate a 3D expression map of MAMs-related genes across the brain following EA intervention. Such studies aim to provide a more robust principled basis for EA as a potential treatment for PD.

5. Conclusions

EA at GV20 and GB34 alleviates PD motor deficits by restoring MAMs' integrity. Mechanistically, EA enhances MAMs function via modulating *Fnl* to improve neuronal organelle interactions and DA homeostasis. This study first demonstrates EA's neuroprotection through MAMs' remodeling, suggesting a multi-target strategy for PD. Targeting *Fnl*-mediated networks may offer novel therapeutic avenues for neurodegeneration.

Availability of Data and Materials

The transcriptome assembled for this study are available on the NCBI Sequence Read Archive via accession number PRJNA1175895 (<https://www.ncbi.nlm.nih.gov/Taxes/study/?acc=PRJNA1175895>).

Author Contributions

PL: Data curation, writing – original draft. FW: Conceptualization. ZF: Investigation, data curation. JL: Visualization. QL: Methodology, investigation. XC: Investigation. SH: Investigation. XQ: Investigation. ZZ: Investigation. YH: Conceptualization, writing - review & editing. JZ: Investigation, writing - review & editing, resources, funding acquisition. All authors contributed to editorial changes in the manuscript. All authors read and ap-

proved the final manuscript. All authors have participated sufficiently in the work and agreed to be accountable for all aspects of the work.

Ethics Approval and Consent to Participate

This study was conducted in accordance with the NIH Guidelines for the Care and Use of Animals and was approved by the Experimental Animal Ethics Committee of Southern Medical University (Approval No. L2021119).

Acknowledgment

Not applicable.

Funding

This research was funded by Natural Science Foundation of Guangdong Province (2021A1515011518); Science and Technology Program of Guangzhou (202102080301); National Natural Science Foundation of China (82305365).

Conflict of Interest

The authors declare no conflict of interest.

Supplementary Material

Supplementary material associated with this article can be found, in the online version, at <https://doi.org/10.31083/JIN40105>.

References

- [1] Cheng Y, Tong Q, Yuan Y, Song X, Jiang W, Wang Y, *et al.* α -Synuclein induces prodromal symptoms of Parkinson's disease via activating TLR2/MyD88/NF- κ B pathway in Schwann cells of vagus nerve in a rat model. *Journal of Neuroinflammation*. 2023; 20: 36. <https://doi.org/10.1186/s12974-023-02720-1>.
- [2] Kalia LV, Lang AE. Parkinson's disease. *Lancet* (London, England). 2015; 386: 896–912. [https://doi.org/10.1016/S0140-6736\(14\)61393-3](https://doi.org/10.1016/S0140-6736(14)61393-3).
- [3] Tysnes OB, Storstein A. Epidemiology of Parkinson's disease. *Journal of Neural Transmission* (Vienna, Austria: 1996). 2017; 124: 901–905. <https://doi.org/10.1007/s00702-017-1686-y>.
- [4] Dong-Chen X, Yong C, Yang X, Chen-Yu S, Li-Hua P. Signaling pathways in Parkinson's disease: molecular mechanisms and therapeutic interventions. *Signal Transduction and Targeted Therapy*. 2023; 8: 73. <https://doi.org/10.1038/s41392-023-01353-3>.
- [5] Angelopoulou E, Stanitsa E, Karpodini CC, Bougea A, Kontaxopoulou D, Fragkiadaki S, *et al.* Pharmacological and Non-Pharmacological Treatments for Depression in Parkinson's Disease: An Updated Review. *Medicina* (Kaunas, Lithuania). 2023; 59: 1454. <https://doi.org/10.3390/medicina59081454>.
- [6] Armstrong MJ, Okun MS. Diagnosis and Treatment of Parkinson Disease: A Review. *JAMA*. 2020; 323: 548–560. <https://doi.org/10.1001/jama.2019.22360>.
- [7] Ma L, Ma L, Yang Y, Chen T, Wang L, Deng Q. Electroacupuncture-Regulated miR-34a-3p/PDCD6 Axis Promotes Post-Spinal Cord Injury Recovery in Both *In Vitro* and *In Vivo* Settings. *Journal of Immunology Research*. 2022; 2022: 9329494. <https://doi.org/10.1155/2022/9329494>.
- [8] Fan JQ, Lu WJ, Tan WQ, Feng WC, Zhuang LX. Acupuncture for Parkinson's disease: From theory to practice. *Biomedicine & Pharmacotherapy*. 2022; 149: 112907. <https://doi.org/10.1016/j.biopha.2022.112907>.
- [9] Xu Y, Cai X, Qu S, Zhang J, Zhang Z, Yao Z, *et al.* Madopar combined with acupuncture improves motor and non-motor symptoms in Parkinson's disease patients: A multicenter randomized controlled trial. *European Journal of Integrative Medicine*. 2020; 34: 101049. <https://doi.org/10.1016/j.eujim.2019.101049>.
- [10] Wang M, Ma C, Liu A, Xiao H, Ren Y, Li Z, *et al.* A bibliometric analysis of acupuncture for Parkinson's disease non-motor symptoms from 2003 to 2023. *Complementary Therapies in Medicine*. 2024; 87: 103111. <https://doi.org/10.1016/j.ctim.2024.103111>.
- [11] Zhao Y, Zhang Z, Qin S, Fan W, Li W, Liu J, *et al.* Acupuncture for Parkinson's Disease: Efficacy Evaluation and Mechanisms in the Dopaminergic Neural Circuit. *Neural Plasticity*. 2021; 2021: 9926445. <https://doi.org/10.1155/2021/9926445>.
- [12] Zhao Y, Luo D, Ning Z, Rong J, Lao L. Electro-Acupuncture Ameliorated MPTP-Induced Parkinsonism in Mice via TrkB Neurotrophic Signaling. *Frontiers in Neuroscience*. 2019; 13: 496. <https://doi.org/10.3389/fnins.2019.00496>.
- [13] Lee Y, Lee H, Bae CH, Seo JE, Kim HY, Koo S, *et al.* Electroacupuncture at GB34 modulates neurogenesis and BDNF-ERK signaling in a mouse model of Parkinson's disease. *Journal of Traditional and Complementary Medicine*. 2023; 13: 263–269. <https://doi.org/10.1016/j.jtcme.2023.01.005>.
- [14] Park J, Oh JY, Park HJ. Potential role of acupuncture in the treatment of Parkinson's disease: A narrative review. *Integrative Medicine Research*. 2023; 12: 100954. <https://doi.org/10.1016/j.imr.2023.100954>.
- [15] Wei TH, Hsieh CL. Effect of Acupuncture on the p38 Signaling Pathway in Several Nervous System Diseases: A Systematic Review. *International Journal of Molecular Sciences*. 2020; 21: 4693. <https://doi.org/10.3390/ijms21134693>.
- [16] Kwon S, Seo BK, Kim S. Acupuncture points for treating Parkinson's disease based on animal studies. *Chinese Journal of Integrative Medicine*. 2016; 22: 723–727. <https://doi.org/10.1007/s11655-016-2525-y>.
- [17] Kim JH, Choi Y, Kim JS, Lee H, Ju IG, Yoo NY, *et al.* Stimulation of microneedles alleviates pathology of Parkinson's disease in mice by regulating the CD4+/CD8+ cells from the periphery to the brain. *Frontiers in Immunology*. 2024; 15: 1454102. <https://doi.org/10.3389/fimmu.2024.1454102>.
- [18] Huo YX, Li XL, Liu W, Wang L, Fan ZX, Kang YZ, *et al.* Study on the regularity of acupoint selection and compatibility of acupuncture and moxibustion in the treatment of Parkinson's disease based on complex network analysis. *Zhen Ci Yan Jiu = Acupuncture Research*. 2024; 49: 1333–1342. <https://doi.org/10.13702/j.1000-0607.20240086>. (In Chinese)
- [19] Sun Z, Jia J, Gong X, Jia Y, Deng J, Wang X, *et al.* Inhibition of glutamate and acetylcholine release in behavioral improvement induced by electroacupuncture in parkinsonian rats. *Neuroscience Letters*. 2012; 520: 32–37. <https://doi.org/10.1016/j.neulet.2012.05.021>.
- [20] Jang JH, Yeom MJ, Ahn S, Oh JY, Ji S, Kim TH, *et al.* Acupuncture inhibits neuroinflammation and gut microbial dysbiosis in a mouse model of Parkinson's disease. *Brain, Behavior, and Immunity*. 2020; 89: 641–655. <https://doi.org/10.1016/j.bbi.2020.08.015>.
- [21] Duan Y, Wang X, Sun K, Lin Y, Wang X, Chen K, *et al.* SYNJB2BP Improves the Production of Lentiviral Envelope Protein by Facilitating the Formation of Mitochondrion-Associated Endoplasmic Reticulum Membrane. *Journal of Virology*. 2022; 96: e0054922. <https://doi.org/10.1128/jvi.00549-22>.
- [22] Paillusson S, Gomez-Suaga P, Stoica R, Little D, Gissen P, Devine MJ, *et al.* α -Synuclein binds to the ER-mitochondria tethering protein VAPB to disrupt Ca^{2+} homeostasis and mito-

- chondrial ATP production. *Acta Neuropathologica*. 2017; 134: 129–149. <https://doi.org/10.1007/s00401-017-1704-z>.
- [23] Markovinic A, Greig J, Martín-Guerrero SM, Salam S, Paillasson S. Endoplasmic reticulum-mitochondria signaling in neurons and neurodegenerative diseases. *Journal of Cell Science*. 2022; 135: jcs248534. <https://doi.org/10.1242/jcs.248534>.
- [24] Erustes AG, Guarache GC, Guedes EDC, Leão AHFF, Pereira GJDS, Smaili SS. α -Synuclein Interactions in Mitochondria-ER Contacts: A Possible Role in Parkinson's Disease. *Contact* (Thousand Oaks (Ventura County, Calif.)). 2022; 5: 25152564221119347. <https://doi.org/10.1177/25152564221119347>.
- [25] Erustes AG, D'Eletto M, Guarache GC, Ureshino RP, Bincolletto C, da Silva Pereira GJ, *et al*. Overexpression of α -synuclein inhibits mitochondrial Ca^{2+} trafficking between the endoplasmic reticulum and mitochondria through MAMs by altering the GRP75-IP3R interaction. *Journal of Neuroscience Research*. 2021; 99: 2932–2947. <https://doi.org/10.1002/jnr.24952>.
- [26] Peng Y, Zhou L, Jin Y, Wu D, Chen N, Zhang C, *et al*. Calcium bridges built by mitochondria-associated endoplasmic reticulum membranes: potential targets for neural repair in neurological diseases. *Neural Regeneration Research*. 2025; 20: 3349–3369. <https://doi.org/10.4103/NRR.NRR-D-24-00630>.
- [27] Basso V, Marchesan E, Ziviani E. A trio has turned into a quartet: DJ-1 interacts with the IP3R-Grp75-VDAC complex to control ER-mitochondria interaction. *Cell Calcium*. 2020; 87: 102186. <https://doi.org/10.1016/j.ceca.2020.102186>.
- [28] Zhang JR, Shen SY, Shen ZQ, Yin SY, Ye K, Li W, *et al*. Role of mitochondria-associated membranes in the hippocampus in the pathogenesis of depression. *Journal of Affective Disorders*. 2024; 361: 637–650. <https://doi.org/10.1016/j.jad.2024.06.076>.
- [29] Maekawa S, Wang PC, Chen SC. Comparative Study of Immune Reaction Against Bacterial Infection From Transcriptome Analysis. *Frontiers in Immunology*. 2019; 10: 153. <https://doi.org/10.3389/fimmu.2019.00153>.
- [30] Wan K, Jia M, Zhang H, Lan Y, Wang S, Zhang K, *et al*. Electroacupuncture Alleviates Neuropathic Pain by Suppressing Ferroptosis in Dorsal Root Ganglion via SAT1/ALOX15 Signaling. *Molecular Neurobiology*. 2023; 60: 6121–6132. <https://doi.org/10.1007/s12035-023-03463-z>.
- [31] Hu ML, Zhu HM, Zhang QL, Liu JJ, Ding Y, Zhong JM, *et al*. Exploring the Mechanisms of Electroacupuncture-Induced Analgesia through RNA Sequencing of the Periaqueductal Gray. *International Journal of Molecular Sciences*. 2017; 19: 2. <https://doi.org/10.3390/ijms19010002>.
- [32] Hu R, He K, Chen B, Chen Y, Zhang J, Wu X, *et al*. Electroacupuncture promotes the repair of the damaged spinal cord in mice by mediating neurocan-perineuronal net. *CNS Neuroscience & Therapeutics*. 2024; 30: e14468. <https://doi.org/10.1111/cns.14468>.
- [33] Hegdekar N, Lipinski MM, Sarkar C. N-Acetyl-L-leucine improves functional recovery and attenuates cortical cell death and neuroinflammation after traumatic brain injury in mice. *Scientific Reports*. 2021; 11: 9249. <https://doi.org/10.1038/s41598-021-88693-8>.
- [34] Koch MS, Zdioruk M, Nowicki MO, Griffith AM, Aguilar E, Aguilar LK, *et al*. Systemic high-dose dexamethasone treatment may modulate the efficacy of intratumoral viral oncolytic immunotherapy in glioblastoma models. *Journal for Immunotherapy of Cancer*. 2022; 10: e003368. <https://doi.org/10.1136/jitc-2021-003368>.
- [35] Arifin WN, Zahiruddin WM. Sample Size Calculation in Animal Studies Using Resource Equation Approach. *The Malaysian Journal of Medical Sciences*. 2017; 24: 101–105. <https://doi.org/10.21315/mjms2017.24.5.11>.
- [36] Zhang X, Song D, Gu L, Ren Y, Verkhatsky A, Peng L. Decrease of gene expression of astrocytic 5-HT_{2B} receptors parallels development of depressive phenotype in a mouse model of Parkinson's disease. *Frontiers in Cellular Neuroscience*. 2015; 9: 388. <https://doi.org/10.3389/fncel.2015.00388>.
- [37] Zhang XL, Hu MN, Rong Z, Li YN, Wang Y, Ma J. Effect of electroacupuncture on Nrf2/NLRP3/Caspase-1 pathway mediated-pyroptosis in mice with Parkinson's disease. *Zhen Ci Yan Jiu = Acupuncture Research*. 2024; 49: 15–22. <https://doi.org/10.13702/j.1000-0607.20230407>.
- [38] Li R, Chen J. Salidroside Protects Dopaminergic Neurons by Enhancing PINK1/Parkin-Mediated Mitophagy. *Oxidative Medicine and Cellular Longevity*. 2019; 2019: 9341018. <https://doi.org/10.1155/2019/9341018>.
- [39] Shiotsuki H, Yoshimi K, Shimo Y, Funayama M, Takamatsu Y, Ikeda K, *et al*. A rotarod test for evaluation of motor skill learning. *Journal of Neuroscience Methods*. 2010; 189: 180–185. <https://doi.org/10.1016/j.jneumeth.2010.03.026>.
- [40] Huang D, Wang Z, Tong J, Wang M, Wang J, Xu J, *et al*. Long-term Changes in the Nigrostriatal Pathway in the MPTP Mouse Model of Parkinson's Disease. *Neuroscience*. 2018; 369: 303–313. <https://doi.org/10.1016/j.neuroscience.2017.11.041>.
- [41] Nemutlu Samur D, Akçay G, Yıldırım S, Özkan A, Çeker T, Derin N, *et al*. Vortioxetine ameliorates motor and cognitive impairments in the rotenone-induced Parkinson's disease via targeting TLR-2 mediated neuroinflammation. *Neuropharmacology*. 2022; 208: 108977. <https://doi.org/10.1016/j.neuropharm.2022.108977>.
- [42] Yan B, Li Y, Min S, Zhang P, Xu B, Wang Z, *et al*. Effects of the Bone/Bone Marrow Microenvironments on Prostate Cancer Cells and CD59 Expression. *BioMed Research International*. 2020; 2020: 2753414. <https://doi.org/10.1155/2020/2753414>.
- [43] Jonas RK, Roh E, Montojo CA, Pacheco LA, Rosser T, Silva AJ, *et al*. Risky Decision Making in Neurofibromatosis Type 1: An Exploratory Study. *Biological Psychiatry. Cognitive Neuroscience and Neuroimaging*. 2017; 2: 170–179. <https://doi.org/10.1016/j.bpsc.2016.12.003>.
- [44] Sumi-Akamaru H, Beck G, Shinzawa K, Kato S, Riku Y, Yoshida M, *et al*. High expression of α -synuclein in damaged mitochondria with PLA2G6 dysfunction. *Acta Neuropathologica Communications*. 2016; 4: 27. <https://doi.org/10.1186/s40478-016-0298-3>.
- [45] Zhang QQ, Chen Q, Cao P, Shi CX, Zhang LY, Wang LW, *et al*. AGK2 pre-treatment protects against thioacetamide-induced acute liver failure via regulating the MFN2-PERK axis and ferroptosis signaling pathway. *Hepatobiliary & Pancreatic Diseases International: HBPDI*. 2024; 23: 43–51. <https://doi.org/10.1016/j.hbpd.2023.03.003>.
- [46] Paillasson S, Stoica R, Gomez-Suaga P, Lau DHW, Mueller S, Miller T, *et al*. There's Something Wrong with my MAM; the ER-Mitochondria Axis and Neurodegenerative Diseases. *Trends in Neurosciences*. 2016; 39: 146–157. <https://doi.org/10.1016/j.tins.2016.01.008>.
- [47] Liu Y, Zhu X. Endoplasmic reticulum-mitochondria tethering in neurodegenerative diseases. *Translational Neurodegeneration*. 2017; 6: 21. <https://doi.org/10.1186/s40035-017-0092-6>.
- [48] Nizamutdinov D, Qi X, Berman MH, Dougal G, Dayawansa S, Wu E, *et al*. Transcranial Near Infrared Light Stimulation Improve Cognition in Patients with Dementia. *Aging and Disease*. 2021; 12: 954–963. <https://doi.org/10.14336/AD.2021.0229>.
- [49] Ma Y, Rong Q. Effect of Different MPTP Administration Intervals on Mouse Models of Parkinson's Disease. *Contrast Media & Molecular Imaging*. 2022; 2022: 2112146. <https://doi.org/10.1155/2022/2112146>.
- [50] Franco A, Walton CE, Dang X. Mitochondria Clumping vs. Mitochondria Fusion in CMT2A Diseases. *Life (Basel)*. 2022; 12: 2110. <https://doi.org/10.3390/life12122110>.
- [51] Han S, Nandy P, Austria Q, Siedlak SL, Torres S, Fujioka H, *et al*. Mfn2 Ablation in the Adult Mouse Hippocampus and Cortex

- Causes Neuronal Death. *Cells*. 2020; 9: 116. <https://doi.org/10.3390/cells9010116>.
- [52] Gómez-Suaga P, Pérez-Nievas BG, Glennon EB, Lau DHW, Paillusson S, Mórotz GM, *et al*. The VAPB-PTPIP51 endoplasmic reticulum-mitochondria tethering proteins are present in neuronal synapses and regulate synaptic activity. *Acta Neuropathologica Communications*. 2019; 7: 35. <https://doi.org/10.1186/s40478-019-0688-4>.
- [53] Hayashi T, Rizzuto R, Hajnoczky G, Su TP. MAM: more than just a housekeeper. *Trends in Cell Biology*. 2009; 19: 81–88. <https://doi.org/10.1016/j.tcb.2008.12.002>.
- [54] Barthelson K, Newman M, Lardelli M. Brain transcriptomes of zebrafish and mouse Alzheimer's disease knock-in models imply early disrupted energy metabolism. *Disease Models & Mechanisms*. 2022; 15: dmm049187. <https://doi.org/10.1242/dmm.049187>.
- [55] Lou X, Han X, Jin C, Tian W, Yu W, Ding D, *et al*. SOX2 targets fibronectin 1 to promote cell migration and invasion in ovarian cancer: new molecular leads for therapeutic intervention. *Omics: a Journal of Integrative Biology*. 2013; 17: 510–518. <https://doi.org/10.1089/omi.2013.0058>.
- [56] Liu F, Gao X, Wang J, Gao C, Li X, Li X, *et al*. Transcriptome Sequencing to Identify Transcription Factor Regulatory Network and Alternative Splicing in Endothelial Cells Under VEGF Stimulation. *Journal of Molecular Neuroscience: MN*. 2016; 58: 170–177. <https://doi.org/10.1007/s12031-015-0653-z>.
- [57] Qin Z, Zhou C. HOXA13 promotes gastric cancer progression partially via the FN1-mediated FAK/Src axis. *Experimental Hematology & Oncology*. 2022; 11: 7. <https://doi.org/10.1186/s40164-022-00260-7>.
- [58] Selvakumar GP, Iyer SS, Kempuraj D, Ahmed ME, Thangavel R, Dubova I, *et al*. Molecular Association of Glia Maturation Factor with the Autophagic Machinery in Rat Dopaminergic Neurons: a Role for Endoplasmic Reticulum Stress and MAPK Activation. *Molecular Neurobiology*. 2019; 56: 3865–3881. <https://doi.org/10.1007/s12035-018-1340-1>.
- [59] Ren Y, Liu W, Zhang J, Bi J, Fan M, Lv Y, *et al*. Corrigendum: MFG-E8 maintains cellular homeostasis by suppressing endoplasmic reticulum stress in pancreatic exocrine acinar cells. *Frontiers in Cell and Developmental Biology*. 2023; 10: 1121052. <https://doi.org/10.3389/fcell.2022.1121052>.
- [60] Khoshdel F, Mottaghi-Dastjerdi N, Yazdani F, Salehi S, Ghorbani A, Montazeri H, *et al*. CTGF, FN1, IL-6, THBS1, and WISP1 genes and PI3K-Akt signaling pathway as prognostic and therapeutic targets in gastric cancer identified by gene network modeling. *Discover Oncology*. 2024; 15: 344. <https://doi.org/10.1007/s12672-024-01225-4>.
- [61] Li X, Yang JY, Hu WZ, Ruan Y, Chen HY, Zhang Q, *et al*. Mitochondria-associated membranes contribution to exercise-mediated alleviation of hepatic insulin resistance: Contrasting high-intensity interval training with moderate-intensity continuous training in a high-fat diet mouse model. *Journal of Diabetes*. 2024; 16: e13540. <https://doi.org/10.1111/1753-0407.13540>.
- [62] Li M, Zhang Y, Yu G, Gu L, Zhu H, Feng S, *et al*. Mitochondria-associated endoplasmic reticulum membranes tethering protein VAPB-PTPIP51 protects against ischemic stroke through inhibiting the activation of autophagy. *CNS Neuroscience & Therapeutics*. 2024; 30: e14707. <https://doi.org/10.1111/cns.14707>.
- [63] Zhou T, Zhang Y, Zheng S, Wang F, Jiang S, Lei W, *et al*. hsa_circ_0051428 Facilitates the Progression of Thyroid Cancer by Sponging miR-1248 to Up-Regulate FN1. *Critical Reviews in Eukaryotic Gene Expression*. 2023; 33: 25–38. <https://doi.org/10.1615/CritRevEukaryotGeneExpr.2022044777>.
- [64] Larrañaga-SanMiguel A, Bengoa-Vergniory N, Flores-Romero H. Crosstalk between mitochondria-ER contact sites and the apoptotic machinery as a novel health meter. *Trends in Cell Biology*. 2025; 35: 33–45. <https://doi.org/10.1016/j.tcb.2024.08.007>.